

Data-driven diffusion-based super-resolution for improvement of reduced-order model predictions in fluid dynamics

Ruan F. S. Sousa

Systems Engineering and Computer Science - COPPE

Federal University of Rio de Janeiro

Rio de Janeiro, Brazil

ruanfelipe@cos.ufrj.br

Roberto M. Velho

Systems Engineering and Computer Science - COPPE

Federal University of Rio de Janeiro

Rio de Janeiro, Brazil

robertovelho@cos.ufrj.br

Natanael L. de Matos

Systems Engineering and Computer Science - COPPE

Federal University of Rio de Janeiro

Rio de Janeiro, Brazil

natanael@cos.ufrj.br

Adriano M. A. Cortes

Systems Engineering and Computer Science - COPPE

Federal University of Rio de Janeiro

Rio de Janeiro, Brazil

adricortes@cos.ufrj.br

Gabriel F. Barros

Civil Engineering - COPPE

Federal University of Rio de Janeiro

Rio de Janeiro, Brazil

gabriel.barros@coc.ufrj.br

Alvaro L. G. A. Coutinho

Civil Engineering - COPPE

Federal University of Rio de Janeiro

Rio de Janeiro, Brazil

alvaro@coc.ufrj.br

Abstract—Computational fluid dynamics simulations provide high-fidelity results but at significant computational cost, creating demand for efficient alternatives. While data-driven surrogate models offer substantial acceleration, they often introduce numerical artifacts and reduced accuracy, particularly when predicting flow patterns for parameters outside training ranges. We address these limitations by proposing a novel two-stage approach that combines a reduced-order modeling (ROM) technique with a denoising diffusion probabilistic model for super-resolution enhancement. Our methodology leverages identical high-fidelity training data for both models, enabling the super-resolution component to effectively denoise and enhance the surrogate model predictions. We demonstrate this approach on the Lock-exchange problem, a benchmark case for sediment transport in incompressible flows. Quantitative evaluation shows consistent improvement across multiple error and image quality metrics compared to standard ROM predictions. The method exhibits robust performance for both interpolation and extrapolation test cases, successfully preserving important flow structures while eliminating numerical artifacts.

Index Terms—Super-resolution, Generative Models, Diffusion probabilistic model, Lock-exchange problem

I. INTRODUCTION

Super-resolution (SR) approaches seek to enhance images that are only available at lower quality due to various constraints. Surrogate models strive to replicate physical system

This study was financed in part by CAPES, Brazil Finance Code 001. This work is also partially supported by FAPERJ, CNPq, and Petrobras.

dynamics while accepting a certain error margin. Their advantage lies in reduced computational complexity, enabling faster processing compared to full high-fidelity dynamic calculations. Contemporary machine learning techniques for fluid flow surrogates have demonstrated exceptional effectiveness, as documented in [1].

The data used to train these surrogates may be low-fidelity due to offline computational limitations, which typically results in lower-quality predictions. Consequently, various methodologies can be employed to enhance such prediction quality. A recently introduced approach by [2] aims to regenerate high-fidelity images (comparable to those produced by Direct Numerical Simulation - DNS) from low-fidelity predictions of turbulent fluid flows generated through techniques such as Large Eddy Simulations (LES), Reynolds Averaged Navier-Stokes (RANS), their hybrid implementation RANS-LES, or functional sub-grid models.

Our methodology distinguishes itself from previous approaches by integrating machine learning-based surrogate models with a super-resolution technique adapted from [2]. We focus specifically on developing surrogate models for parametric fluid flow systems, which are typically governed by systems of partial differential equations (PDEs). A comprehensive description of our surrogate model construction methodology follows the work of [3] and [4] and can be found in a preprint by several co-authors of the current work [5].

Our primary objective is to accurately reproduce fluid flow

dynamics governed by the relevant equation system for parameters not encountered during training. The innovation in our approach lies in utilizing the surrogate model's predictions as inputs to a pre-trained super-resolution framework, generating outputs with better accuracy compared to ground truth (test data) than would be achievable with surrogate predictions alone. To achieve this synergistic effect, the super-resolution model must be trained using the same dataset employed for training the surrogate model.

To validate our methodology, we selected the Lock-exchange problem [6], a well-documented and experimentally validated configuration for studying sediment transport in turbulent fluid flows. We employed a Finite Element Method solver to discretize the coupled PDE system, generating a comprehensive dataset of high-fidelity simulations. These solutions, referred to as the Full Order Model (FOM), served dual purposes: they provided the foundation for training and validating the surrogate model while simultaneously enabling the development and testing of the super-resolution model that enhances the surrogate predictions.

The next sections are structured as follows: In the Methodology section, we present the Lock-exchange problem configuration, including the governing equations, boundary conditions, and other parameters related to the continuous formulation, followed by a concise overview of the reduced-order methodology employed for surrogate model generation. We then outline the dataset generation process and conclude with the super-resolution methodology, which is founded on the Denoising Diffusion Probabilistic Model (DDPM) framework. The Results section provides a detailed analysis of our experiments coupling both data-driven models and an evaluation of their performance according to established metrics. Finally, in the Conclusion section, we summarize our findings and discuss future research directions in this domain.

II. METHODOLOGY

In this section, we describe the Lock-exchange problem formulation, the process of generating data for training and testing the SR model, its theoretical aspects and its application.

A. Lock-Exchange Problem Setup

The lock-exchange problem is a fundamental benchmark for investigating density-driven flows and sediment transport phenomena. Our configuration consists of a two-dimensional inclined rectangular channel with non-dimensionalized dimensions $L_x = 18$ and $L_y = 2$. Initially, the domain is partitioned at $x = 0$: the left section (with width $L_x^0 = 1$ and $L_y^0 = 2$) is filled with sediment-laden fluid, while the right section contains clear fluid (Fig. 1). The inclination of the channel is parameterized by a θ angle, measured with respect to the x -axis. The system is modeled using the Navier–Stokes

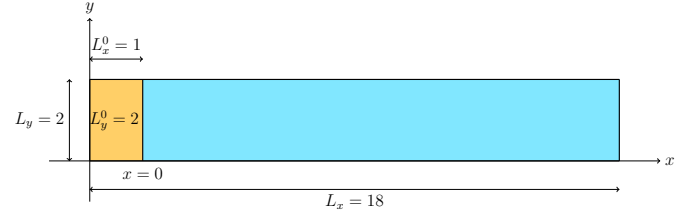


Fig. 1. Lock-Exchange problem initial setup for $\theta = 0^\circ$.

equations in non-dimensional form in their non-conservative formulation:

$$\frac{\partial \mathbf{u}}{\partial t} + \mathbf{u} \cdot \nabla \mathbf{u} = -\nabla p + \frac{1}{\sqrt{Gr}} \Delta \mathbf{u} + c \mathbf{e}_\theta^g, \quad (1a)$$

$$\nabla \cdot \mathbf{u} = 0, \quad (1b)$$

$$\frac{\partial c}{\partial t} + (\mathbf{u} + u_S \mathbf{e}_\theta^g) \cdot \nabla c = \nabla \cdot \left(\frac{1}{Sc\sqrt{Gr}} \nabla c \right). \quad (1c)$$

Here, c denotes the normalized sediment concentration (defined as C/C_0 , with C being the current concentration and C_0 a reference concentration), \mathbf{u} is the velocity field, p is the pressure, and u_S represents the constant sedimentation velocity. The non-dimensional parameters include the Grashof number Gr and the Schmidt number Sc . The Grashof number (Gr) quantifies the ratio of buoyancy to viscous forces, while the Schmidt number (Sc) measures the relative rates of momentum and mass transport. The gravitational force is incorporated through the term $c \mathbf{e}_\theta^g$, where the unit vector $\mathbf{e}_\theta^g = (\sin \theta, -\cos \theta)$ defines the direction of gravity, with θ being the channel's inclination angle.

Boundary conditions enforce a no-slip condition ($\mathbf{u} = \mathbf{0}$) on all solid boundaries (top, bottom, and vertical sides) and a zero-flux Neumann condition for sediment concentration ($\partial c / \partial n = 0$, where $\partial / \partial n$ denotes the normal derivative) to ensure mass conservation by preventing sediment exchange with walls. Initially, a sharp concentration interface exists at $x = 0$ with $c = 1$ for $x < 0$ and $c = 0$ for $x > 0$, while velocity is zero throughout. Upon simulation start, the denser sediment-laden fluid advances beneath the lighter fluid, generating a gravity current with distinctive head formation and complex interfacial dynamics, up to time T_f .

For the parametric studies, the channel inclination angle θ is varied. This variation alters the gravitational force components and, consequently, the flow dynamics. Notably, the formulation accommodates different inclination angles solely by adjusting the gravitational force direction via the \mathbf{e}_θ^g term, without requiring any modifications to the Cartesian reference system.

B. Surrogate Model

A comprehensive description of our surrogate model construction methodology is available in a preprint by several co-authors of the current work [5]. Due to space constraints, we present only a concise overview here. Since our approach

employs reduced-order methodology, we refer to the surrogate model as ROM (Reduced-Order Model) throughout the remainder of this paper.

The construction of a Reduced-Order Model (ROM) for (1) begins with a high-fidelity approximation via Finite Element Method (FEM) discretization. This high-fidelity discrete full-order model (FOM) represents a nonlinear parameterized dynamical system. For any $\theta \in [0, \theta_{\max}] \subset \mathbb{R}$, we solve:

$$\begin{cases} \dot{\mathbf{v}}_h(t; \theta) = \mathbf{F}(t, \mathbf{v}_h(t; \theta), \theta), & t \in (0, T), \\ \mathbf{v}_h(0; \theta) = \mathbf{v}_0(\theta), \end{cases} \quad (2)$$

where $\mathbf{v}_h = (\mathbf{u}_h, p_h, c_h) \in \mathbb{R}^{N_u} \times \mathbb{R}^{N_p} \times \mathbb{R}^{N_\phi}$ represents the discrete fields, $\mathbf{v}_h : [0, T] \times [0, \theta_{\max}] \rightarrow \mathbb{R}^{N_h}$ is the parameterized solution with $N_h = N_u + N_p + N_c$, \mathbf{F} encodes the system dynamics, and \mathbf{v}_0 denotes the initial condition.

The solution manifold for this system, defined as

$$\mathcal{S}_h = \{\mathbf{v}_h(t; \theta) \mid t \in [0, T] \text{ and } \theta \in [0, \theta_{\max}]\} \subset \mathbb{R}^{N_h}, \quad (3)$$

is fundamental to ROM development. Despite \mathcal{S}_h residing in an N_h -dimensional space, its intrinsic dimension is at most $2 \ll N_h$. This dimensional disparity creates both an opportunity and a challenge: each solution point $\mathbf{v}_h(t; \theta)$ can be described by few coordinates, but \mathcal{S}_h remains a nonlinear manifold embedded in high-dimensional space.

Our data-driven, non-intrusive ROM methodology comprises two distinct phases. The offline phase involves three steps incorporating two machine learning tasks: (1) generating high-dimensional FOM simulation data across parameter and time variations; (2) applying dimensionality reduction (PCA followed by an Autoencoder) to map this data to an appropriate latent space; and (3) training a regression model on the reduced data to learn the temporal and parametric dynamics of state variables in latent coordinates. The online phase leverages these machine learning outputs: for new time instances and parameters, we evaluate the regression model to predict latent coefficients, then reconstruct the high-dimensional solution in physical space. This approach effectively exploits the low intrinsic dimensionality of the solution manifold while managing its nonlinear structure. Finally, it is worth to note that, because of the non-intrusiveness of the approach, we can build a surrogate model for each of the physical fields. In our case, we focused on the sediment concentration.

C. Dataset Generation and Processing

Due to the turbulent nature of the flow characterized by Grashof number $Gr = 5.0 \times 10^6$ and Schmidt number $Sc = 1.0$, we employed a Stabilized FEM formulation. Specifically, we implemented the residual-based variational multiscale method (RBVMS) [7] for equation (1) using the FEniCS 2019.1 framework [8].

Our computational domain was discretized with a fixed mesh of 701×101 nodes and 700×100 cells, each divided into two linear triangles, yielding $N_c = 70801$ concentration values. We set the final simulation time to $T_f = 22$ and employed an Implicit Euler time-stepping scheme with a fixed

step size of $\Delta t = 0.05$. The channel inclination angle θ was varied from 0° to $\theta_{\max} = 10^\circ$ in 2° increments for training purposes. Additionally, we solved cases at $\theta = 5^\circ$ and $\theta = 12^\circ$ to serve as interpolation and extrapolation test cases, respectively.

The training dataset (snapshot matrix) was constructed by collecting concentration field data at 440 time instants for each training angle, organized in ascending angle order. The matrix columns are arranged sequentially: first, all time steps for $\theta = 0^\circ$ from $t = 0.05$ to $t = 22.0$, followed by all time steps for $\theta = 2^\circ$, and so on through $\theta = 10^\circ$. This arrangement produced a matrix of dimensions 70801×2640 ($= 6$ angles \times 440 time steps), where each column represents a concentration field vector at a specific angle and time. Fig. 2 shows the concentration field for different times and angles parameter.

This training dataset serves as the foundation for both the surrogate model and the super-resolution model which will be described in the next section.

D. Description of the Super-resolution model

Before proceeding, we note that we have maintained standard notation conventions from the literature. Consequently, some mathematical symbols used previously may reappear in a different context. We believe this should pose no difficulty for readers, as these symbols operate within entirely separate domains.

The super-resolution method described here is based on a denoising diffusion probabilistic model (DDPM). DDPMs are Markov chain-based generative models that aim to learn the distribution $p_{data}(x)$ of a dataset to generate new samples conforming to this distribution. To learn $p_{data}(x)$, the model applies a forward process where a sample $x \sim p_{data}$ undergoes sequential addition of random noise until it is transformed into Gaussian noise. Subsequently, in the reverse process, the model learns to systematically remove each added noise component, reconstructing the original image as illustrated in Fig. 3.

Given a dataset of samples from $p_{data}(x)$, with each sample denoted by x_0 , we construct a sequence of T latent representations $\{x_1, \dots, x_T\}$ through Gaussian transitions defined as:

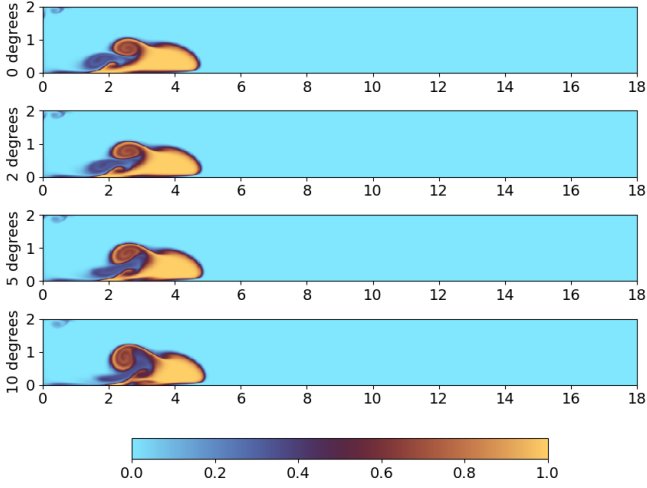
$$q(x_t | x_{t-1}) = \mathcal{N}\left(x_t; \sqrt{1 - \beta_t}x_{t-1}, \beta_t I\right), \quad (4)$$

where β_1, \dots, β_T is a progressive variance scaling factor that approaches 1 as t approaches T , ensuring that $x_T \sim \mathcal{N}(0, I)$. This is called the forward diffusion process.

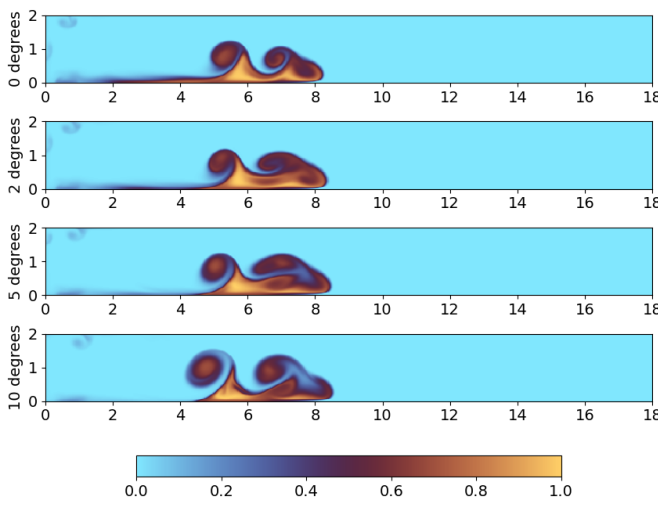
The Markovian assumption gives us the factorization:

$$q(x_{1:T} | x_0) = \prod_{t=1}^T q(x_t | x_{t-1}). \quad (5)$$

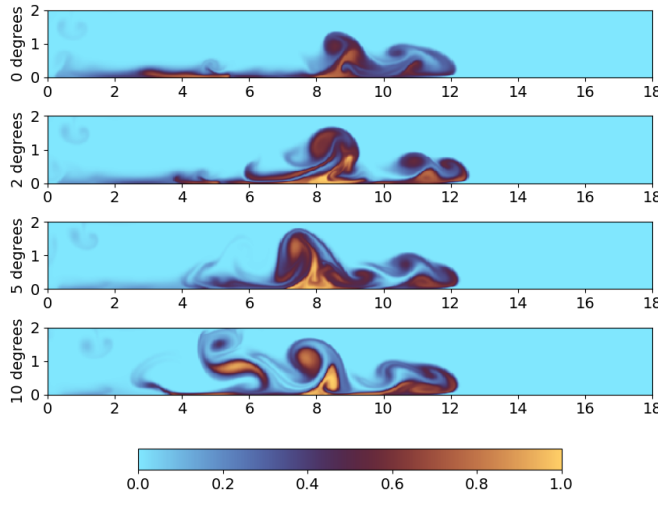
The model aims to learn the reverse process $p_\theta(x_{0:T})$, which is defined as a Markov chain with learned Gaussian transitions starting at $p_\theta(x_T)$, where $x_T \sim \mathcal{N}(x_T; 0, I)$ and θ represents the learnable neural network parameters. This process can be interpreted as establishing a stochastic mapping



(a)



(b)



(c)

Fig. 2. FOM sediment concentration evolution in the lock exchange configuration. Each figure shows four slopes for the channel angles of 0, 2, 5, and 10 degrees. Channel dimensions are length $L_x = 18$ and height $L_y = 2$; (a), (b) and (c) Sediment concentration at $t = 6.25$, $t = 12.5$, and $t = 22$ respectively.

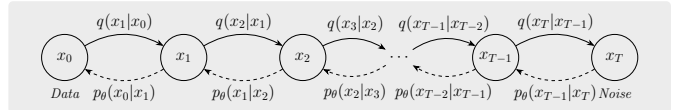


Fig. 3. Markovian process in DDPM showing forward diffusion q and reverse denoising p_θ transitions.

between the standard Gaussian distribution and the target data distribution.

For a data sample x_0 to be reconstructed, the reconstruction procedure, i.e. the reverse denoising process, can be formulated as:

$$p_\theta(x_{0:T}) = p(x_T) \prod_{t=1}^T p_\theta(x_{t-1}|x_t), \quad (6)$$

where T is the number of steps in the diffusion process. The probability transition $p_\theta(x_{t-1}|x_t)$ is modeled as a Gaussian distribution:

$$p_\theta(x_{t-1}|x_t) = \mathcal{N}(x_{t-1}; \mu_\theta(x_t, t), \Sigma_\theta(x_t, t)), \quad (7)$$

where $\mathcal{N}(x; \mu, \beta I)$ represents a Gaussian kernel with mean μ and variance βI , with I being the identity matrix. The transition functions μ_θ and Σ_θ are learned during the model training process.

The ideal loss function to minimize would be the negative log-likelihood, $-\log p_\theta(x_0)$. However, this expression is not directly tractable. Instead, following the approach of [9], we minimize the evidence lower bound (ELBO), which provides a tractable approximation. This derivation results in the following loss function:

$$\begin{aligned} L_t &= \mathbb{E}_{t \sim [1, T], x_0, \epsilon} \left[\|\epsilon_t - \epsilon_\theta(x_t, t)\|^2 \right] \\ &= \mathbb{E}_{t \sim [1, T], x_0, \epsilon} \left[\|\epsilon_t - \epsilon_\theta(\sqrt{\alpha_t} x_0 + \sqrt{1 - \alpha_t} \epsilon_t, t)\|^2 \right] \end{aligned} \quad (8)$$

where $\alpha_t = 1 - \beta_t$, $\bar{\alpha}_t = \prod_{i=1}^t \alpha_i$, and $\epsilon_t \sim \mathcal{N}(0, I)$ is the standard Gaussian noise sampled at time t . The term $\epsilon_\theta(\cdot, \cdot)$ represents the model's predicted noise given x_t and t as inputs. Intuitively, this loss function trains the model to estimate the noise component added at each diffusion step, allowing for its removal during the reverse process. The training and sampling algorithms based on [9] are presented here in Algorithms 1 and 2, respectively.

Algorithm 1 Training

- 1: **repeat**
 - 2: $\mathbf{x}_0 \sim q(\mathbf{x}_0)$
 - 3: $t \sim \text{Uniform}(\{1, \dots, T\})$
 - 4: $\boldsymbol{\epsilon} \sim \mathcal{N}(\mathbf{0}, \mathbf{I})$
 - 5: Take gradient descent step on
 - 6: $\nabla_\theta \|\boldsymbol{\epsilon} - \epsilon_\theta(\sqrt{\alpha_t} \mathbf{x}_0 + \sqrt{1 - \alpha_t} \boldsymbol{\epsilon}, t)\|^2$
 - 7: **until** converged
-

Algorithm 2 Sampling

```

1:  $\mathbf{x}_T \sim \mathcal{N}(\mathbf{0}, \mathbf{I})$ 
2: for  $t = T, \dots, 1$  do
3:    $\mathbf{z} \sim \mathcal{N}(\mathbf{0}, \mathbf{I})$  if  $t > 1$ , else  $\mathbf{z} = \mathbf{0}$ 
4:    $\mathbf{x}_{t-1} = \frac{1}{\sqrt{\alpha_t}} \left( \mathbf{x}_t - \frac{1-\alpha_t}{\sqrt{1-\bar{\alpha}_t}} \epsilon_\theta(\mathbf{x}_t, t) \right) + \sigma_t \mathbf{z}$ 
5: end for
6: return  $\mathbf{x}_0$ 
  
```

E. Application of the Technique

The training of the super-resolution model, with a linear schedule for β_t from $\beta_1 = 10^{-4}$ to $\beta_T = 0.02$ and $T = 1000$, was performed using an NVIDIA A400 GPU for 300 epochs, requiring approximately 16 hours of computation time. We utilized the implementation from [10] associated with [2], developed in the PyTorch framework. The training employed the ADAM optimizer with a constant learning rate of 2×10^{-4} and a batch size of 12.

For evaluation, we applied the trained diffusion super-resolution model to the ROM outputs for angles not included in the training set. A critical consideration in this process is that ROM output is not Gaussian noise; rather, it already contains the principal characteristics expected in the final solution. Consequently, we cannot input the ROM at the final step of the diffusion chain ($T = 1000$) for denoising. Instead, we must introduce it at an intermediate step $n_s < T$ of the chain to facilitate appropriate noise removal.

This starting step of the reverse process serves as a hyperparameter of our super-resolution method and governs the degree of denoising applied. When the selected starting time is insufficient, the Enhanced ROM results exhibit numerous numerical artifacts, indicating inadequate denoising. Conversely, an excessively large starting time can lead to over-correction, potentially eliminating smaller secondary dynamics and resulting in information loss. Through empirical testing, we determined that a starting time of $n_s = 200$ produces optimal reconstruction quality. Developing a predictor for this hyperparameter remains an objective for future work.

III. RESULTS

To evaluate the effectiveness of our approach, we analyze the performance of both the ROM and Enhanced ROM (via super-resolution) on two test cases: $\theta = 5^\circ$, which represents an interpolation within the parameter range used for training, and $\theta = 12^\circ$, which represents an extrapolation outside this parameter range. Importantly, the full-order solutions for both angles were not included in the training datasets.

Fig. 4 and 5 present the visual comparison between the ROM and Enhanced ROM predictions for angles $\theta = 5^\circ$ and $\theta = 12^\circ$, respectively. In both test cases, the Enhanced ROM demonstrates a good improvement in solution quality compared to the standard ROM. The super-resolution model effectively removes noise and numerical artifacts present in the ROM predictions, highlighting its denoising capabilities. Notably, for the interpolation case ($\theta = 5^\circ$), we observe

that the Enhanced ROM successfully preserves important secondary flow structures while eliminating numerical artifacts. This selective enhancement indicates that the super-resolution model correctly distinguishes between physical flow features and numerical noise. For the extrapolation case ($\theta = 12^\circ$), despite being outside the parameter range used during training, the Enhanced ROM still provides significant improvements over the standard ROM predictions. This demonstrates the robust generalization capability of our approach beyond the training parameter space.

We employed several quantitative metrics to assess prediction accuracy. The relative l_2 norm is defined as the ratio between the l_2 norm of the prediction error and the l_2 norm of the full-order solution, that is, relative $l_2 = \frac{\|x_{\text{pred}} - x_{\text{FOM}}\|_2}{\|x_{\text{FOM}}\|_2}$. We also utilize the l_∞ norm, which represents the maximum absolute error between the predicted and full-order solutions, identifying the largest point-wise discrepancy. Additionally, we employed image quality metrics: the Peak Signal-to-Noise Ratio (PSNR), which measures the quality of reconstruction by quantifying the ratio between the maximum possible power of the signal and the power of corrupting noise, and the Structural Similarity Index Measure (SSIM), a perceptual metric that quantifies image quality degradation caused by processing, providing insight into preserved structural information. For both PSNR and SSIM calculations, we utilized the implementation available in the scikit-image library [11].

We evaluated both models across the entire time interval of the flow dynamics to assess their temporal consistency. Fig. 6a and 6b present the evolution of the quantitative metrics over time for the interpolation and extrapolation cases, respectively. The temporal analysis reveals that the Enhanced ROM consistently outperforms the standard ROM throughout the simulation period for both test cases, with a larger improvement for the interpolation angle than for the extrapolation one. This persistent improvement suggests that our super-resolution approach enhances not only individual snapshots but also maintains the coherence of the dynamic evolution of the flow field.

The Enhanced ROM achieves lower relative l_2 and l_∞ error norms while demonstrating higher PSNR and SSIM values compared to the standard ROM. This comprehensive improvement across multiple metrics confirms the effectiveness of our approach in enhancing the accuracy of reduced-order modeling predictions.

IV. CONCLUSIONS

The integration of diffusion-based super-resolution with reduced-order modeling provides quantifiable improvements in solution accuracy, with consistent reductions in relative l_2 and l_∞ error norms. Our Enhanced ROM demonstrates superior performance on both interpolated ($\theta = 5^\circ$) and extrapolated ($\theta = 12^\circ$) test cases, with higher PSNR and SSIM values compared to standard ROM predictions. The super-resolution component successfully differentiates between physical flow structures and numerical artifacts, preserving essential secondary dynamics while removing noise. The optimal start-

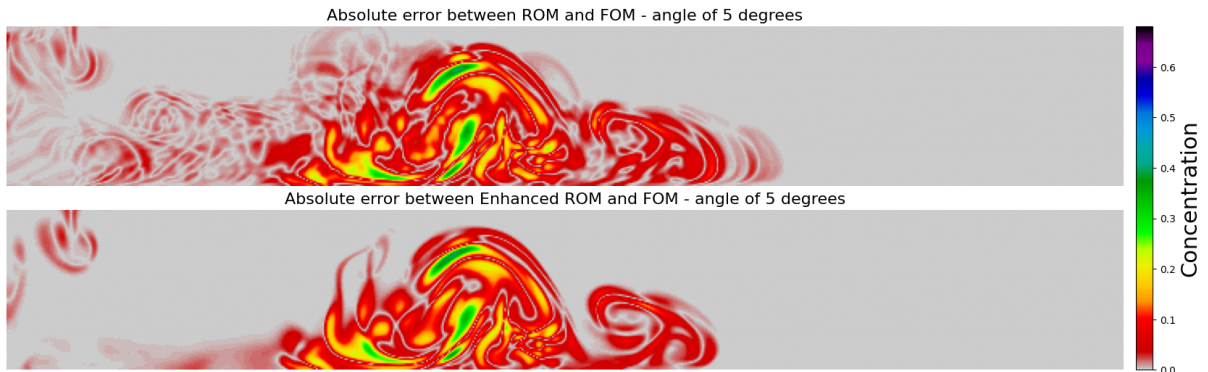
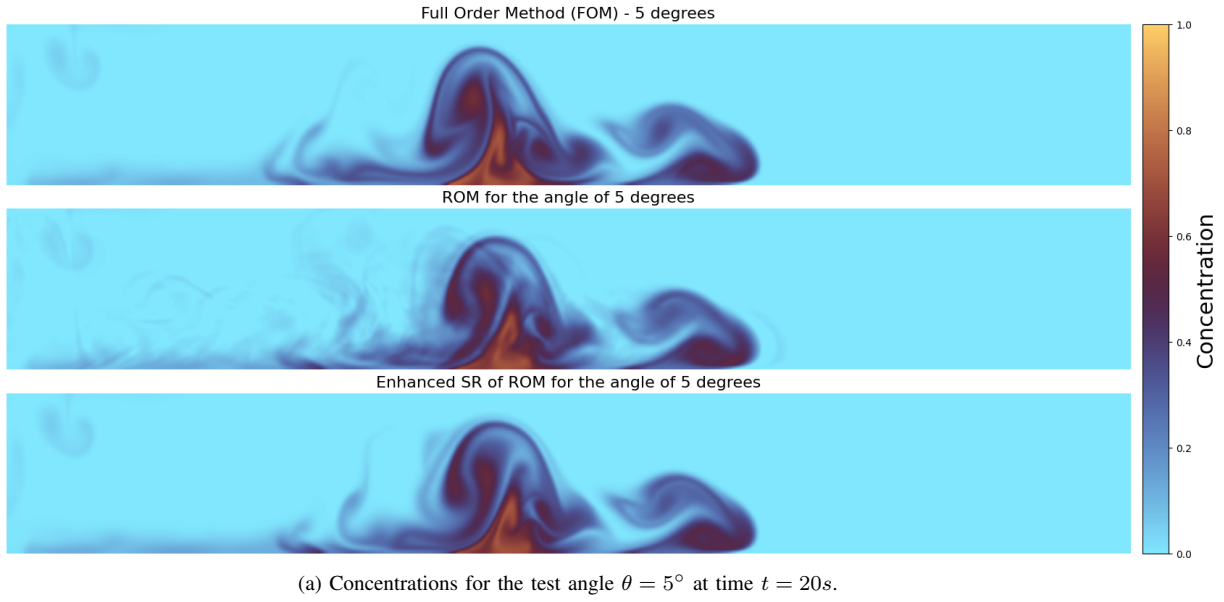


Fig. 4. Results for the test angle $\theta = 5^\circ$.

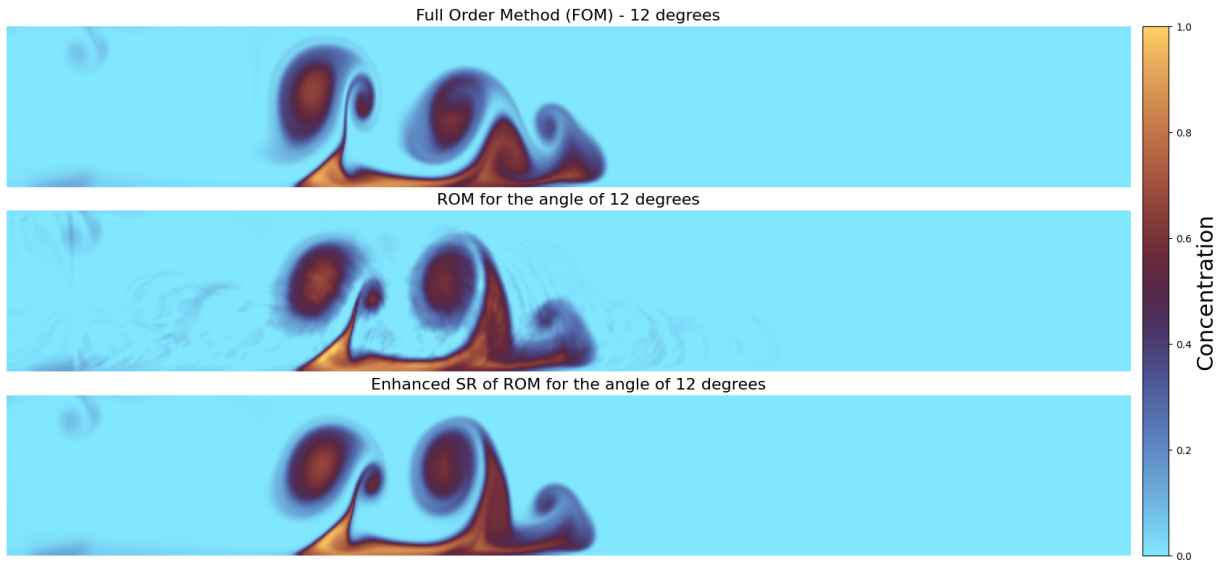
ing time parameter for the reverse diffusion process was empirically determined to be $n_s = 200$, balancing artifact removal against overcorrection. The combined approach maintains temporal consistency of flow dynamics throughout the simulation period, not merely enhancing individual snapshots. The methodology remains effective even for parameter values beyond the training range, indicating robust generalization capabilities. Future developments will focus on automatic selection criteria for diffusion hyperparameters and incorporating physics-informed constraints into the generation process to ensure adherence to conservation laws and physical principles.

Authorship statement. The authors hereby confirm that they are the sole liable persons responsible for the authorship of this work, and that all material that has been herein included as part of the present paper is either the property (and authorship) of the authors, or has the permission of the owners to be included here.

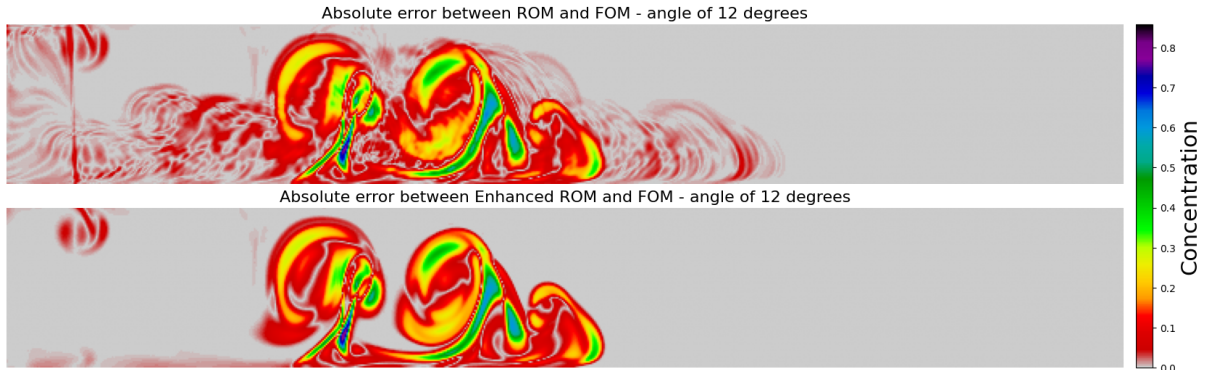
REFERENCES

- [1] R. Vinuesa and S. L. Brunton, “Enhancing computational fluid dynamics with machine learning,” *Nature Computational Science*, vol. 2, no. 6, pp.

- 358–366, 2022.
- [2] D. Shu, Z. Li, and A. Barati Farimani, “A physics-informed diffusion model for high-fidelity flow field reconstruction,” *Journal of Computational Physics*, vol. 478, p. 111972, Apr. 2023. [Online]. Available: <http://dx.doi.org/10.1016/j.jcp.2023.111972>
- [3] M. Guo and J. S. Hesthaven, “Data-driven reduced order modeling for time-dependent problems,” *Computer Methods in Applied Mechanics and Engineering*, vol. 345, 2018.
- [4] S. Fresca and A. Manzoni, “Pod-dl-rom: Enhancing deep learning-based reduced order models for nonlinear parametrized pdes by proper orthogonal decomposition,” *Computer Methods in Applied Mechanics and Engineering*, vol. 388, 2022.
- [5] R. Velho, A. Córtes, G. Barros, F. Rochinha, and A. Coutinho, “Advances in data-driven reduced order models using two-stage dimension reduction for coupled viscous flow and transport,” *Preprint*, 2024, https://papers.ssrn.com/sol3/papers.cfm?abstract_id=5064259.
- [6] E. Meiburg and B. Kneller, “Turbidity currents and their deposits,” *Annual review of fluid mechanics*, vol. 42, no. 1, pp. 135–156, 2010.
- [7] G. M. Guerra, S. Zio, J. J. Camata, F. A. Rochinha, R. N. Elias, P. L. Parizo, and A. L. Coutinho, “Numerical simulation of particle-laden flows by the residual-based variational multiscale method,” *International Journal for Numerical Methods in Fluids*, vol. 73, no. 8, pp. 729–749, 2013.
- [8] M. S. Alnæs, J. Blechta, J. Hake, A. Johansson, B. Kehlet, A. Logg, C. Richardson, J. Ring, M. E. Rognes, and G. N. Wells, “The fenics project version 1.5,” *Archive of Numerical Software*, vol. 3, no. 100, 2015.



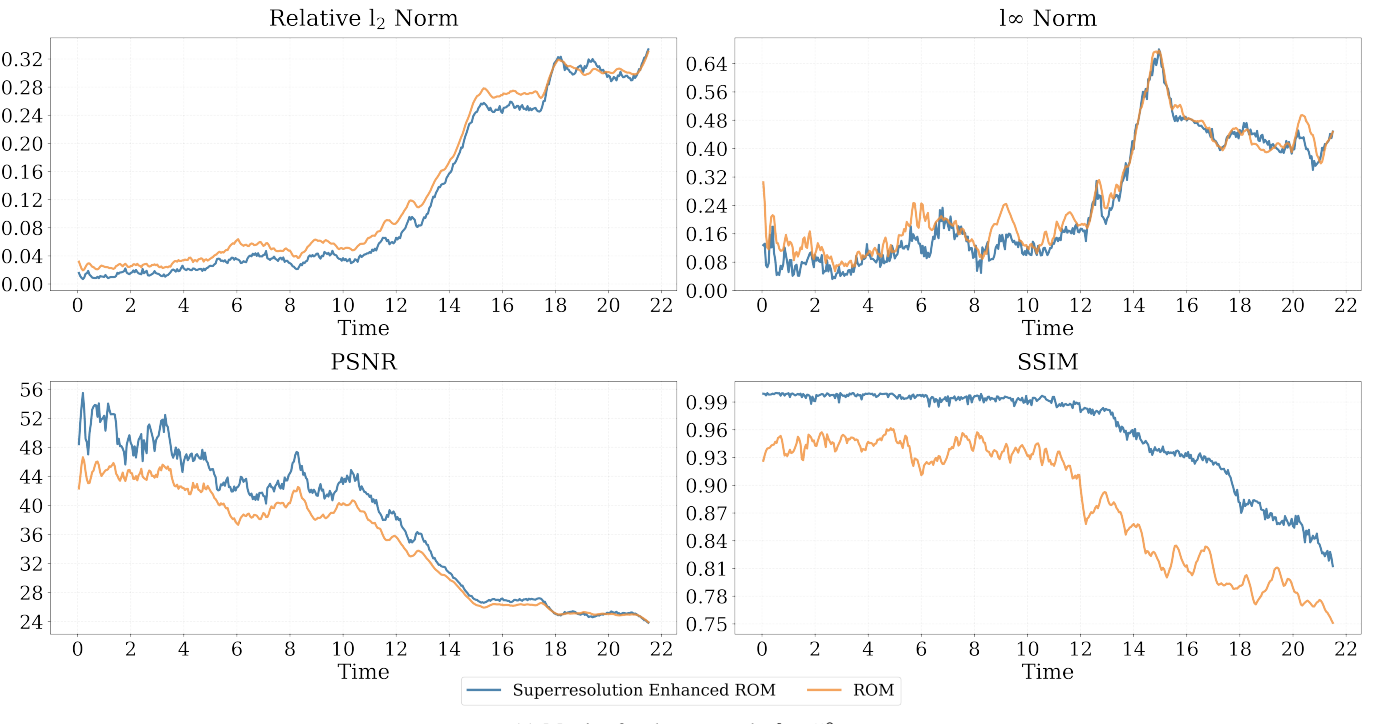
(a) Concentrations for the test angle $\theta = 12^\circ$ at time $t = 15s$.



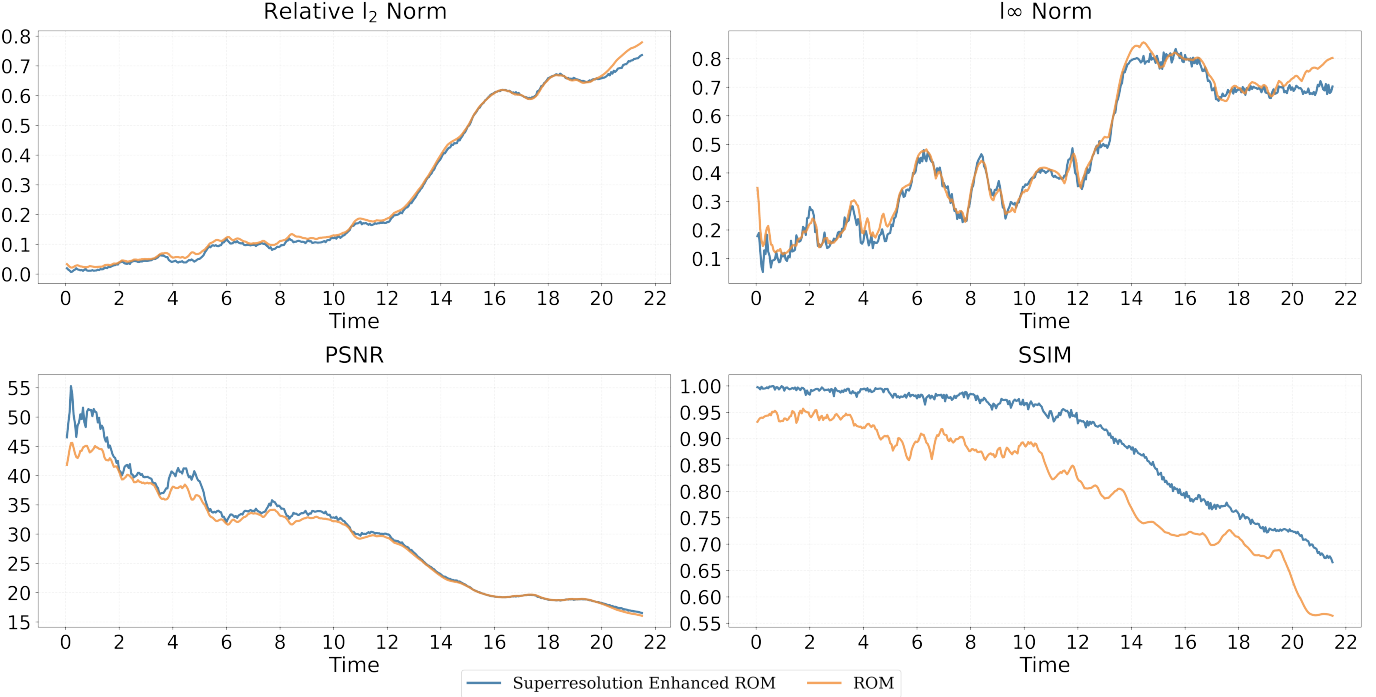
(b) Absolute error for the test angle $\theta = 12^\circ$ at time $t = 15s$.

Fig. 5. Results for the test angle $\theta = 12^\circ$.

- [9] J. Ho and T. Salimans, “Classifier-free diffusion guidance,” *arXiv:2207.12598*, 2022. [Online]. Available: <https://arxiv.org/abs/2207.12598>
- [10] D. Shu, Z. Li, and A. B. Farimani, “Diffusion-based-fluid-super-resolution,” 2023. [Online]. Available: https://github.com/BaratiLab/Diffusion-based-Fluid-Super-resolution/tree/main_v1
- [11] S. van der Walt, J. L. Schönberger, J. Nunez-Iglesias, F. Boulogne, J. D. Warner, N. Yager, E. Gouillart, T. Yu, and the scikit-image contributors, “scikit-image: image processing in Python,” *PeerJ*, vol. 2, p. e453, 6 2014. [Online]. Available: <https://doi.org/10.7717/peerj.453>



(a) Metrics for the test angle $\theta = 5^\circ$.



(b) Metrics for the test angle $\theta = 12^\circ$.

Fig. 6.